THE JOURNAL OF PHYSICAL CHEMISTRY C

pubs.acs.org/JPCC Article

High-Pressure Tetrahedral Amorphous Carbon Synthesized by Compressing Glassy Carbon at Room Temperature

Lijie Tan, Hongwei Sheng, Hongbo Lou, Benyuan Cheng, Yuanyuan Xuan, Vitali B. Prakapenka, Eran Greenberg, Qiaoshi Zeng, Fang Peng, and Zhidan Zeng*

Cite This: J. Phys. Chem. C 2020, 124, 5489−5494

Read Online

ACCESS | Metrics & More | Article Recommendations

ABSTRACT: Tetrahedral amorphous carbon(ta-C) thin films with high sp^3 fraction have extraordinary mechanical properties and wide applications. Despite intensive effort to increase the thickness of ta-C thin films in the past decades, bulk ta-C has not been achieved until date. In this study, by compressing a sp^2-bonded amorphous carbon (glassy carbon) up to 93 GPa, we demonstrate that the formation of bulk ta-C is possible at high pressures and room temperature. We studied the atomic structure, stability, and mechanical properties of the ta-C synthesized under high pressure using in situ high-pressure X-ray diffraction and large-scale first-principles calculations. The high-pressure ta-C is mainly tetrahedrally bonded, with relatively large distortions in the sp^3 C−C bonds. It can be preserved to approximately 8.5 GPa during pressure release, below which it transforms to disordered glassy carbon, accompanied by sp^3-to-sp^2 transition. Moreover, both the experiment and simulation show that the high-pressure ta-C has a high bulk modulus (363 ± 29 GPa, experimental) even comparable to diamond. These results deepen our understanding of amorphous carbon and help guide the synthesis of novel carbon materials using high pressure.

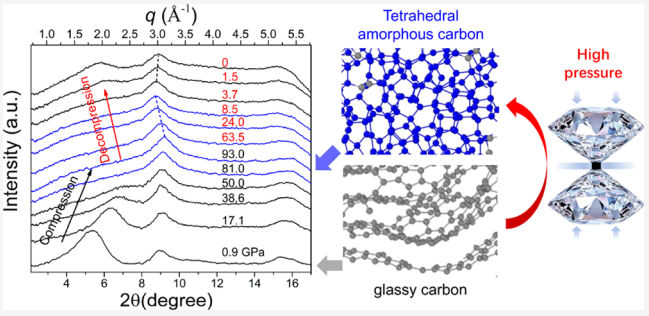

1. INTRODUCTION

Carbon forms a great variety of crystalline and disordered structures owing to its flexibility in bonding (sp^1-, sp^2-, and sp^3-hybridized bonds). Among the numerous carbon allotropes, those with a high fraction of sp^3 bonds usually have extraordinary mechanical properties. Therefore, carbon materials with high sp^3 fraction, not only in crystalline but also in amorphous forms, have been extensively studied.[1−3] Amorphous carbon with very high sp^3 fraction (up to ∼88%) contains a high percentage of tetrahedral bonding and is named tetrahedrally bonded amorphous carbon (ta-C).[2] Currently, ta-C is only available in the form of thin films, which are usually grown using various film deposition techniques involving energetic ions or plasma beams.[2] The typical thickness of ta-C films was reported to range from a few to tens of nanometers.[2,4,5] However, the ta-C thin films have extraordinary mechanical properties, chemical inertness, thermal stability, and large band gap, hence wide applications.[2,4,5] Considerable efforts have been devoted to increasing its thickness.[6,7] However, to the best of our knowledge, bulk (three dimensional) ta-C has not been achieved until date.

Pressure has been proved to be a powerful tool to induce sp^2-to-sp^3 bonding transition in sp^2-bonded carbon materials.[8−12] Glassy carbon (GC), a mostly sp^2 bonded amorphous carbon allotrope,[13] was also found to undergo structural and bonding transitions under pressure.[10,14−16] Utilizing the effect of pressure, various sp^3-bonded carbon forms have been synthesized by high-pressure and high-temperature (HPHT) treatment of GC, for example, nanocrystalline diamond, hexagonal diamond, and recently discovered amorphous diamond.[17−19] In addition to HPHT, pressure-induced transitions have also been observed in cold-compressed (at room temperature) GC. The sp^2-to-sp^3 bonding transition in cold-compressed GC was observed in in situ high-pressure X-ray Raman scattering experiments[10] and in molecular dynamics and first-principles simulations.[14,15,20] This transition was confirmed in various experiments with dramatic changes in Raman spectrum, mechanical strength, optical properties, and electrical properties of GC.[10,18,21,22] In contrast to the consistent results on the property transitions of GC mentioned above, the structural description of these transitions remains in a state of flux. In situ high-pressure X-ray diffraction (XRD) experiments, up to 47 or 51.4 GPa, revealed that GC went through structural transition during compression without a

Received: January 10, 2020
Published: February 6, 2020

https://dx.doi.org/10.1021/acs.jpcc.0c00247
J. Phys. Chem. C 2020, 124, 5489−5494

pressure-transmitting medium.[22,23] However, complete transition has not been observed in these experiments because of limited pressure ranges applied. Moreover, a recent high-pressure pair distribution function (PDF) study on the cold-compressed GC reported that GC maintains its original graphite-like structure up to 49.0 GPa.[24] Therefore, a couple of intriguing questions are raised: Does a complete transition exist in cold compression? How high is the pressure required to synthesize a pure high-pressure phase of GC? How stable will the high-pressure phase be? These questions call for further experimental studies.

In this work, by combining in situ high-pressure XRD up to 93 GPa and first-principles calculations up to ~200 GPa, we observed a complete transformation of GC into high-pressure ta-C under cold compression. The atomic structure, stability, and compressibility of the ta-C formed under high pressure were thoroughly investigated. Our results demonstrate that ta-C can be synthesized at room temperature with the aid of high pressure and clarify the structure of the cold-compressed GC.

2. EXPERIMENTS AND SIMULATION

In situ high-pressure XRD experiments were carried out at beamline 13 ID-D of the advanced photon source (APS), Argonne National Laboratory (ANL), USA. The X-ray has a wavelength of 0.3220 Å and was focused down to ~3 μm × 3 μm. A MAR165 charge-coupled device detector was used for data collection, and the software DIOPTAS was used to integrate the two-dimensional diffraction images.[25] A symmetric diamond anvil cell (DAC) with culet sizes of ~200 μm was used. The GC sample (type I, from Alfa Aesar) with a thickness of ~40 μm was loaded into an 80 μm diameter hole drilled in a Re gasket. To maximize the sample thickness for better signal, no pressure medium was used in our experiments. A membrane system was used to increase and decrease pressure. A tiny piece of Au foil was loaded along with the sample as the pressure standard. The pressure was determined using the equation of state of Au.[26] Background scattering from the diamond anvils was collected before loading the sample and subtracted to obtain XRD patterns of the sample.

First-principles calculations based on the Vienna Ab initio Simulation Package (VASP) were performed to derive the detailed atomic structure of GC during compression to ~200 GPa and decompression.[27] The simulation method is similar to what we used to investigate the phase transition mechanism of GC under high pressure.[19] To recapitulate, liquid carbon was quenched with a fixed density of 2.1 g/cm^3 from 5000 to 1000 K at a cooling rate of 5 × 10^{13} K/s using ab initio molecular dynamics simulation to obtain GC. The radial distribution function and the structure factor, $S(q)$, were calculated based on a large structure model of GC with 1024 atoms. The simulations were carried out in a canonical ensemble (NVT) with each time step representing 2 fs. The temperature was controlled with the Nosé−Hoover thermostat.[27] The projector-augmented wave potential with a valence configuration of 2s2p and the generalized gradient approximation were used for C in the simulation.[28] To account for the van der Waals correction, the optB86b-vdW functional from the nonlocal exchange−correlation functions was used.[29] To simulate hydrostatic compression and decompression of GC, the simulation box size was scaled with small steps, followed by conjugate gradient geometric optimization to achieve the minimum energy state of the structure. As a consequence of the different stress conditions between experiments and simulation, the phase transition pressure in simulation is much higher than that in experiments.

3. RESULTS AND DISCUSSION

Figure 1 shows representative XRD patterns of the GC sample during compression to 93 GPa and following decompression to

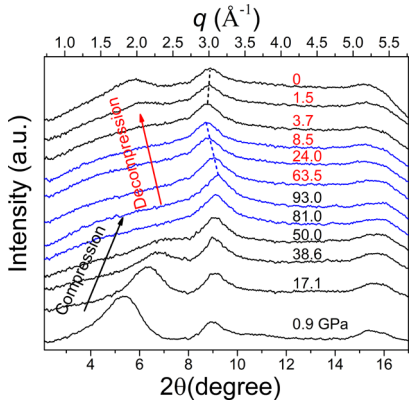

Figure 1. In situ high-pressure XRD of GC. XRD patterns of GC at representative pressures during compression up to 93 GPa and decompression to 0 GPa. The patterns of the high-pressure phase are shown in blue. No pressure medium was used in the experiment in order to generate high deviatoric stress. The X-ray wavelength is 0.3220 Å. The dashed lines serve as a guide to the eye. The numbers on each pattern are the pressures where the patterns were collected.

0 GPa. The XRD pattern of the GC shows two broad characteristic peaks, the first diffraction peak (FDP) and the second diffraction peak (SDP), corresponding to the average interlayer and intralayer characteristic distances in GC, respectively. As shown in Figure 1, with increasing pressure, the FDP becomes extremely weak at 50 GPa and eventually disappears at 81 GPa. Meanwhile, the SDP of GC seems to become stronger during compression. These changes in the XRD patterns indicate that a structural transition occurs in GC during compression, and the transition has completed at ~81 GPa. Therefore, at 81 GPa, we obtained the XRD pattern of the pure high-pressure phase for the first time, without contributions from the original GC phase. It should be noted that because of the layered feature of the structure of GC, development of a strong texture in GC could also result in intensity weakening or even disappearance of the FDP,[14,23] similar to the disappearance of (002) peak in uniaxially compressed graphite as a result of the strong texture. If the intensity change of the FDP was dominated by the texture, the FDP could not re-appear because the texture once formed during compression by plastic anisotropy will remain in decompression mainly with elastic recovery. However, as shown in Figure 1, the FDP reappears upon full decompression. Therefore, we conclude that the disappearance of the FDP should be dominated by reversible phase transitions.

The XRD pattern of the high-pressure phase shows a main peak at ~3.1 Å^{-1} at 81 GPa, and it shifts to ~2.96 Å^{-1} when decompressed to 8.5 GPa. The position of the main peak is quite similar to that of ta-C (main peak at ~2.9 Å^{-1} at 0 GPa) and amorphous diamond (main peak at ~2.95 Å^{-1} at 0 GPa) which mainly consist of the tetrahedral network structure and sp^3 bonds.[3,19] Therefore, it is most likely that the high-pressure phase observed in this work has an atomic structure similar to ta-C with high content of sp^3-bonds, and we name it high-

https://dx.doi.org/10.1021/acs.jpcc.0c00247
J. Phys. Chem. C 2020, 124, 5489−5494

pressure ta-C (ta-C for short in the remaining text unless otherwise specified). The atomic structure, bonding, and properties of this ta-C will be further explored in the following.

The phase transition in GC that completed at ∼81 GPa is consistent with the previous observation that a GC sphere becomes translucent at ∼113 GPa in quasi-uniaxial compression, and the G-band in its Raman spectrum meanwhile disappears.[18] Our previous high-pressure XRD and resistance measurement experiments both suggest that phase transition in GC has not completed up to 61.3 GPa. Therefore, the initial GC phase and the high-pressure phase coexist even at the highest pressure of these experiments, preventing a full understanding of the structure and properties of the high-pressure phase. It should be noted that a recent high-pressure PDF study claims that GC maintains graphite-like structure up to 49 GPa because the derived average C−C−C bond angle is close to that in graphite (120°). Meanwhile, the average coordination number (CN) of C atoms increases from ∼2.67 at ambient pressure to ∼3.5 during compression to 49 GPa, indicating the formation of sp^3 bonds.[24] The discrepancy could be partially attributed to the relatively low pressure reached in their experiment, at which the content of the high-pressure phase is not high enough to be fully recognized. In addition, a large volume cell instead of DAC was used in their study. The different deviatoric stress involved in the experiments could also play an important role because the phase transition in GC is proved to be quite sensitive to shear stress.[18,20,22]

During decompression, the main peak of the ta-C shifts to lower q values smoothly, indicating that ta-C remains stable down to 8.5 GPa. Upon further decompression, a broad peak emerges at ∼2.0 $Å^{-1}$ (where the FDP of GC used to be located) and becomes stronger with decreasing pressure, suggesting the ta-C starts to transform back to GC. This is in line with the fact that the translucent GC sphere under high pressure can be sustained down to at least 17 GPa and became opaque when the pressure was removed.[18] The intensity of FDP in the recovered sample is much lower than that of the initial GC, implying the recovered sample has a substantially more disordered layered structure. In contrast, our previous high-pressure XRD experiment up to 51.4 GPa, at which the phase transition of GC has not completed, the intensity of FDP almost fully recovered upon decompression.[22] It should be noted that, in contrast to the ta-C obtained through cold compression of type-I GC in this study, nanocrystalline sp^3-bonded carbon was observed in cold-compressed type-II GC up to 47 GPa.[23] Also, it reverts to nanocrystalline graphite with a preferred orientation upon decompression,[14] suggesting that various phases can be obtained by compressing disordered carbon materials with different initial atomic structures and transition paths.

To obtain more detailed information on this phase transition, we fit the FDP and SDP of GC to the Gaussian function to obtain their peak positions and intensity as a function of pressure. As shown in Figure 2a, the interlayer distance (corresponding to FDP) shrinks smoothly with increasing pressure. In contrast, the peak position of SDP shows abnormal changes during compression. With increasing pressure, it first decreases when compressed to ∼17.1 GPa, then increases slightly between 26.0 and 50.0 GPa, and decreases again when compressed from 81.0 to 93.0 GPa. These two transitions can be well explained by the GC-to-ta-C phase transition with a sluggish transition zone from ∼26 to around 81 GPa. As shown in Figure 1, the SDP of GC and the

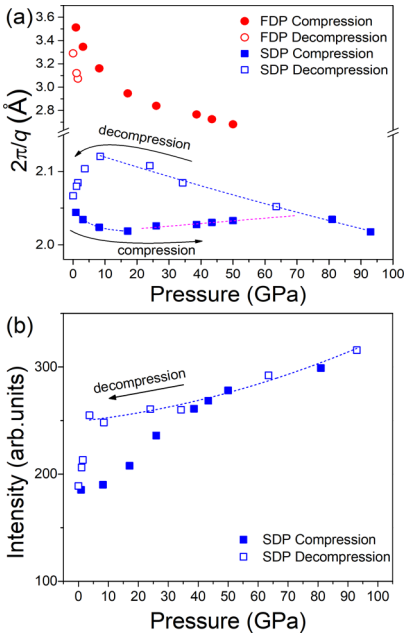

Figure 2. Position (a) and intensity (b) of the FDP (squares) and SDP (circles) of GC as functions of pressure during compression up to 93 GPa (solid symbols) and decompression (open symbols). The peak position and intensity were derived by fitting the diffraction peaks to Gaussian functions. The dashed lines serve as a guide to the eye.

main peak of ta-C are both quite broad and have similar peak positions. Therefore, these two peaks merge into one broad peak located near ∼3.0 $Å^{-1}$ (herein, we still call this peak SDP for consistency) when both GC and ta-C phases are present. As a consequence, when pressure is below 17.1 GPa or above 81.0 GPa, the SDP shifts to higher q (smaller $2\pi/q$) normally with increasing pressure because only one phase (GC or ta-C) is present. In the pressure range of 26.0−50.0 GPa, both phases coexist. The main peak of ta-C is always located at lower q side of the SDP of GC, for example, 2.96 $Å^{-1}$ (ta-C) versus 3.10 $Å^{-1}$ (GC) at approximately 8 GPa. The ta-C content increases gradually with increasing pressure because of sluggish phase transition. Correspondingly, with the increasing interference of the ta-C, the SDP peak position deviates from the original trend and slightly shifts to lower q with increasing pressure in the pressure range of 26.0−50.0 GPa. Moreover, the intensity of SDP increases rapidly with pressure which is consistent with the expectation of transition from sp^2 to sp^3 bonds.

During decompression, a sharp transition in the peak position and intensity of SDP was observed below 8.5 GPa (see Figure 2a,b), indicating that the ta-C can be maintained down to 8.5 GPa, followed by a transition to disordered GC upon full decompression.

Although the in situ high-pressure XRD experiments provide direct experimental evidence of the formation of ta-C upon cold compression of GC, the detailed information of the atomic structure of ta-C is lacking because of the limited q range covered in the experiment and the relative weak signal. First-principles calculations were then employed to derive more detailed information of the ta-C. Figure 3 shows the structure factor ($S(q)$), radial distribution functions ($g(r)$), and bond angle distribution of the simulated GC structure at selected pressures during decompression from 198 GPa, and

https://dx.doi.org/10.1021/acs.jpcc.0c00247
J. Phys. Chem. C 2020, 124, 5489−5494

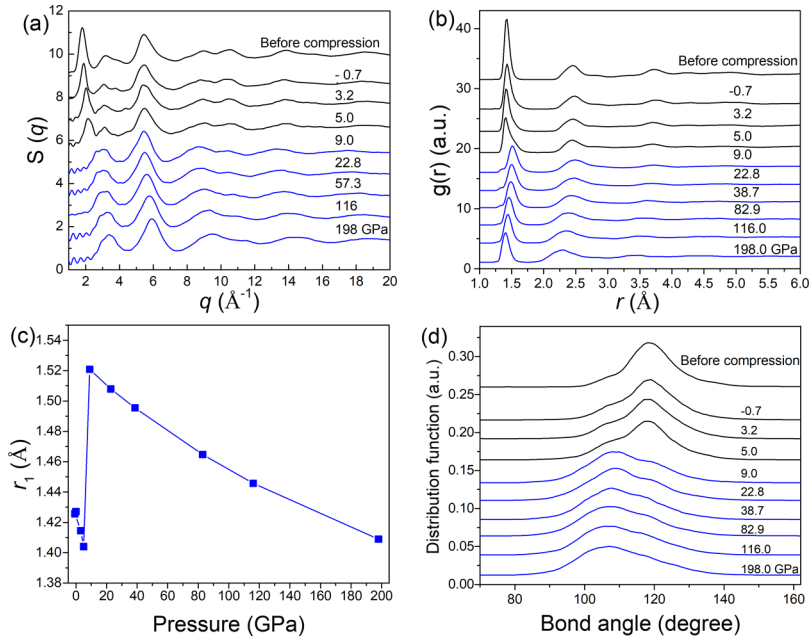

Figure 3. Structure factor $S(q)$ (a), radial distribution functions $g(r)$ (b), position of the first peak of $g(r)(r_1)$ (c), and bond angle distribution (d) of GC as a function of pressure in decompression from 198 GPa. The $S(q)$, $g(r)$, and bond angle distribution of the high-pressure ta-C are shown in blue.

the data of GC before compression were also included for comparison. In our previous simulation, the FDP of GC still exists when it was compressed to 94.6 GPa, although it becomes quite weak.[22] However, our current experiments suggest the transition could be completed when pressure is high enough. Therefore, we further increased the pressure to 198 GPa in the simulation of this study, at which the FDP of GC does completely disappear (see Figure 3a), supporting the experimental results in turn. Meanwhile, the position of the first peak in $g(r)$ which corresponds to the first nearest neighbor C−C distance (r_1), that is, C−C bond length, is 1.41 Å (see Figure 3b,c). The typical C−C bond length in sp^2-bonded carbon is 1.42 Å (according to graphite) and in sp^3-bonded carbon is 1.54 Å (according to diamond) at ambient pressure. Apparently, the bond length 1.41 Å at 198 GPa should be attributed to compressed sp^3 bonds rather than sp^2 bonds. Moreover, the distribution of C−C bond angle shows maximum at approximately 107°, close to the 109.5° in an ideal tetrahedral structure (see Figure 3d). Meanwhile, the bond angle distribution shows a weak shoulder near ∼120°, implying the existence of a small amount of residual sp^2 bonds. The bond length and bond angle distribution of the structure are in full agreement with the sp^3 fraction of 90%, which is derived directly from the average CN of C atoms in the structural model. Therefore, combining experimental and simulation results, we can conclude that the GC has been converted to highly sp^3-bonded ta-C under very high pressure.

During decompression, $S(q)$ does not show obvious change down to 9.0 GPa, except that the peaks shift to lower q because of the elastic recovery of lattice, consistent with our experimental results. Correspondingly, the C−C bond length increases continuously with decreasing pressure (from 1.41 Å at 198 GPa to 1.52 Å at 9.0 GPa), and the bond angle distribution only changes slightly, implying that the ta-C remains quite stable in this pressure range. When the pressure reaches 5.0 GPa, the FDP of GC re-appears in $S(q)$, and the intensity of SDP drops obviously. Meanwhile, a strong peak emerges at ∼1.40 Å in $g(r)$, and the peak at 1.52 Å becomes quite weak and eventually disappears upon further decompression. Also, the center of the bond angle distribution shifts to 119°, quite close to 120° in the graphene or graphite-like structure. The abrupt changes in $S(q)$, $g(r)$, and bond angle all indicate that the sp^3-bonded ta-C has transformed to sp^2-bonded disordered GC during decompression below ∼9 GPa.

Because the ta-C formed under pressure cannot be recovered to ambient pressure, we could not remove it from DAC to measure its mechanical properties at ambient conditions. Instead, by tracking the diffraction peaks (sample volume) of the ta-C as a function of pressure, the elastic compressibility (the inverse of the bulk modulus) could be derived, for example, by fitting the volume change of ta-C during decompression using a second-order Birch−Murnaghan equation of state (BM-EOS) (see Figure 4). The volume change of ta-C is estimated by assuming a cubic power law between the volume and the inverse position of its main diffraction peak (q^{-1}). The bulk modulus derived from the fitting is 363 ± 29 GPa. It should be noted that because high-pressure ta-C cannot be recovered to ambient pressure, V_0 was also fitted along with the bulk modulus. Meanwhile, simulations were also employed to calculate the bulk modulus of ta-C for comparison and validation. The pressure−volume data of ta-C obtained from the simulation were fitted to a second-order BM-EOS as well, and the derived bulk modulus of ta-C near 0 GPa is 300 ± 2 GPa. The EOS of the amorphous diamond, diamond, and GC are also plotted for comparison in Figure 4.[19,30] As shown in Figure 4, both the experimental and simulation results suggest that the ta-C has ultra-high incompressibility even comparable to amorphous diamond (B_0 = 377.6(3) GPa) and diamond (B_0 = 438.1(7) GPa).[19] It is interesting to note that the bulk modulus of high-pressure ta-C is also similar to that of conventional ta-C thin films, which is ∼334 (+111, −54) GPa when sp^3 fraction is 88%.[4] The high bulk modulus of high-pressure ta-C is in line

https://dx.doi.org/10.1021/acs.jpcc.0c00247
J. Phys. Chem. C 2020, 124, 5489−5494

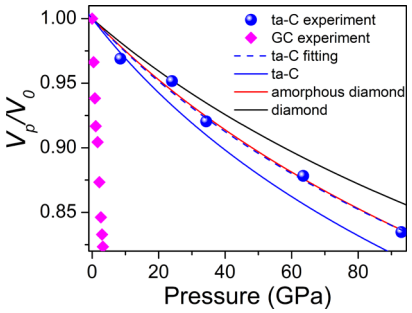

Figure 4. Pressure vs fractional volume changes for GC (purple diamond symbols, experimental results),[30] crystalline diamond (black solid line, simulation results), amorphous diamond (red solid line, simulation results), and the high-pressure ta-C (blue circles for experimental data, blue dashed line for fitting,[19] blue solid line for simulation results). The volume change of ta-C is estimated by assuming a cubic power law between the volume and the inverse position of its main diffraction peak (q^{-1}). The peak position was derived by fitting the diffraction peaks to a Gaussian function, and the error of fitting is smaller than the symbol size.

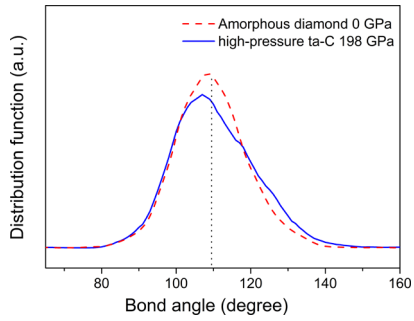

Figure 5. Distribution of the C−C bond angle in the high-pressure ta-C at 198 GPa (solid line) and amorphous diamond at 0 GPa (dashed line) derived from simulation. The dotted line denotes the ideal tetrahedral bond angle of 109.5°.

with its high sp^3 fraction and also with the fact that it can sustain a quite high stress difference, for example, 70 GPa.[10,18]

According to the experimental XRD and simulated $S(q)$ patterns, the high-pressure ta-C seems to have a similar structure with ta-C thin films grown with the aid of energetic ions or plasma beams, and amorphous diamond synthesized under HPHT.[19,31] Although the high-pressure ta-C also features a tetrahedral network structure like the other two amorphous carbon forms, subtle differences still exist. The main difference lies in their stability at ambient conditions. Both ta-C thin films and amorphous diamond are metastable at ambient conditions[7,19] but not the high-pressure ta-C. In the following discussion, we will focus on high-pressure ta-C and amorphous diamond because they are both synthesized under pressure. It is well known that at ambient conditions, graphite is thermodynamically stable, and diamond has slightly higher Gibbs free energy than graphite (by ∼2.5 kJ/mol at 0 K) .[32] However, their relative stability can be reversed by applying pressure, enabling the graphite-to-diamond transition under HPHT. Similarly, although sp^2-bonded amorphous carbon is more stable than sp^3-bonded amorphous carbon at ambient pressure, ta-C with high sp^3 content becomes more energy favorable under high pressure, hence enables the GC-to-ta-C transition. However, for this transition at room temperature, extremely high atomic strain would have been built in ta-C because of the lack of thermally activated atom diffusion and strain relaxation, preventing the ta-C from reaching the local energy minimum. This is rather different from the synthesis of amorphous diamond which takes place under quite high temperature (∼1800 K). As a consequence, the high-pressure ta-C contains highly distorted tetrahedral structure (i.e., distorted strong, directional C−C covalent bonds with an average bond angle obviously deviated from that in the ideal tetrahedral structure as shown in Figure 5) with much higher energy than amorphous diamond,[19] and a fully sp^3-bonded structure could not be obtained even under extremely high pressure, for example, in our simulation, the ta-C formed at 198 GPa still contains approximately 10% sp^2 bonds. When pressure is released, the amorphous diamond can be sustained like diamond, whereas the high-pressure ta-C transforms to disordered GC because of its relatively high free energy.

4. CONCLUSIONS

In summary, by combining in situ high-pressure XRD and large-scale ab initio simulations, we thoroughly investigated phase transition in cold-compressed GC and found that GC completely transformed into a highly sp^3-bonded ta-C at ∼81 GPa. The high-pressure ta-C has a structure similar to that of the recently discovered amorphous diamond and traditional ta-C thin films and can be preserved down to 8.5 GPa during decompression, followed by a transition to GC with a highly disordered structure upon full decompression. As a consequence of high sp^3 fraction, the high-pressure ta-C is extremely incompressible, with a high bulk modulus (363 ± 29 GPa) comparable to diamond. Our results demonstrate that in addition to the extensively studied ta-C thin films, by utilizing high pressure, in principle, it is viable to synthesize bulk high-pressure ta-C through pressure-induced solid-phase transitions. The high-pressure ta-C is expected to have similar mechanical and optical properties with the ta-C films and would have important applications should it be sustained to ambient conditions. These results deepen our understanding of amorphous carbon and may guide the synthesis of novel amorphous carbon materials with desired properties utilizing high pressure.

AUTHOR INFORMATION

Corresponding Author

Zhidan Zeng − *Center for High Pressure Science and Technology Advanced Research (HPSTAR), Shanghai 201203, China*; Email: zengzd@hpstar.ac.cn

Authors

Lijie Tan − *Institute of Atomic and Molecular Physics, Sichuan University, Chengdu 610065, China; Center for High Pressure Science and Technology Advanced Research (HPSTAR), Shanghai 201203, China*; orcid.org/0000-0001-9396-7613

Hongwei Sheng − *Center for High Pressure Science and Technology Advanced Research (HPSTAR), Shanghai 201203, China*

Hongbo Lou − *Center for High Pressure Science and Technology Advanced Research (HPSTAR), Shanghai 201203, China*

Benyuan Cheng − *Center for High Pressure Science and Technology Advanced Research (HPSTAR), Shanghai 201203, China; Shanghai Institute of Laser Plasma, Shanghai 201800, China*

https://dx.doi.org/10.1021/acs.jpcc.0c00247
J. Phys. Chem. C 2020, 124, 5489−5494

Yuanyuan Xuan − *Center for High Pressure Science and Technology Advanced Research (HPSTAR), Shanghai 201203, China*
Vitali B. Prakapenka − *Center for Advanced Radiation Sources, University of Chicago, Chicago, Illinois 60637, United States*
Eran Greenberg − *Center for Advanced Radiation Sources, University of Chicago, Chicago, Illinois 60637, United States*
Qiaoshi Zeng − *Center for High Pressure Science and Technology Advanced Research (HPSTAR), Shanghai 201203, China; Jiangsu Key Laboratory of Advanced Metallic Materials, School of Materials Science and Engineering, Southeast University, Nanjing 211189, People's Republic of China*
Fang Peng − *Institute of Atomic and Molecular Physics, Sichuan University, Chengdu 610065, China*

Complete contact information is available at: https://pubs.acs.org/10.1021/acs.jpcc.0c00247

Notes

The authors declare no competing financial interest.

■ ACKNOWLEDGMENTS

The authors acknowledge the financial support of the National Key R&D Program of China (2018YFA0703404) and the National Natural Science Foundation of China (U1930401, 51871054). The XRD work was performed at the beamline 13-IDD of GSECARS, APS, ANL. GSECARS is supported by NSF (EAR-1634415) and DOE (DE-FG02-94ER14466). APS is supported by DOE-BES under contract no. DE-AC02-06CH11357.

■ REFERENCES

(1) LiBassi, A.; Ferrari, A. C.; Stolojan, V.; Tanner, B. K.; Robertson, J.; Brown, L. M. Density, sp^3 content and internal layering of DLC films by X-ray reflectivity and electron energy loss spectroscopy. *Diamond Relat. Mater.* **2000**, *9*, 771−776.
(2) Robertson, J. Diamond-like amorphous carbon. *Mater. Sci. Eng., R* **2002**, *37*, 129−281.
(3) McKenzie, D. R.; Muller, D.; Pailthorpe, B. A. Compressive-stress-induced formation of thin-film tetrahedral amorphous carbon. *Phys. Rev. Lett.* **1991**, *67*, 773−776.
(4) Ferrari, A. C.; Robertson, J.; Beghi, M. G.; Bottani, C. E.; Ferulano, R.; Pastorelli, R. Elastic constants of tetrahedral amorphous carbon films by surface Brillouin scattering. *Appl. Phys. Lett.* **1999**, *75*, 1893−1895.
(5) Teo, K. B. K.; Ferrari, A. C.; Fanchini, G.; Rodil, S. E.; Yuan, J.; Tsai, J. T. H.; Laurenti, E.; Tagliaferro, A.; Robertson, J.; Milne, W. I. Highest optical gap tetrahedral amorphous carbon. *Diamond Relat. Mater.* **2002**, *11*, 1086−1090.
(6) Friedmann, T. A.; Sullivan, J. P.; Knapp, J. A.; Tallant, D. R.; Follstaedt, D. M.; Medlin, D. L.; Mirkarimi, P. B. Thick stress-free amorphous-tetrahedral carbon films with hardness near that of diamond. *Appl. Phys. Lett.* **1997**, *71*, 3820−3822.
(7) Ferrari, A. C.; Rodil, S. E.; Robertson, J.; Milne, W. I. Is stress necessary to stabilise sp^3 bonding in diamond-like carbon? *Diamond Relat. Mater.* **2002**, *11*, 994−999.
(8) Mao, W. L.; Mao, H.-k.; Eng, P. J.; Trainor, T. P.; Newville, M.; Kao, C.-c.; Heinz, D. L.; Shu, J.; Meng, Y.; Hemley, R. J. Bonding Changes in Compressed Superhard Graphite. *Science* **2003**, *302*, 425.
(9) Wang, Z.; Zhao, Y.; Tait, K.; Liao, X.; Schiferl, D.; Zha, C.; Downs, R. T.; Qian, J.; Zhu, Y.; Shen, T. A quenchable superhard carbon phase synthesized by cold compression of carbon nanotubes. *Proc. Natl. Acad. Sci. U.S.A.* **2004**, *101*, 13699.
(10) Lin, Y.; Zhang, L.; Mao, H.-k.; Chow, P.; Xiao, Y.; Baldini, M.; Shu, J.; Mao, W. L. Amorphous Diamond: A High-Pressure Superhard Carbon Allotrope. *Phys. Rev. Lett.* **2011**, *107*, 175504.
(11) Goncharov, A. F. Graphite at high pressures: Pseudomelting at 44 GPa. *High Pressure Res.* **1992**, *8*, 430−432.
(12) Mao, H.-K.; Chen, B.; Chen, J.; Li, K.; Lin, J.-F.; Yang, W.; Zheng, H. Recent advances in high-pressure science and technology. *Matter Radiat. Extremes* **2016**, *1*, 59.
(13) Harris, P. J. F. Fullerene-related structure of commercial glassy carbons. *Philos. Mag.* **2004**, *84*, 3159−3167.
(14) Shiell, T. B.; et al. Graphitization of Glassy Carbon after Compression at Room Temperature. *Phys. Rev. Lett.* **2018**, *120*, 215701.
(15) Jiang, X.; Århammar, C.; Liu, P.; Zhao, J.; Ahuja, R. The R3-carbon allotrope: a pathway towards glassy carbon under high pressure. *Sci. Rep.* **2013**, *3*, 1877.
(16) Goncharov, A. F. Graphite at high pressure: pseudomelting at 44 GPa. *High Pressure Res.* **1992**, *8*, 430.
(17) Solopova, N. A.; Dubrovinskaia, N.; Dubrovinsky, L. Synthesis of nanocrystalline diamond from glassy carbon balls. *J. Cryst. Growth* **2015**, *412*, 54−59.
(18) Yao, M.; Fan, X.; Zhang, W.; Bao, Y.; Liu, R.; Sundqvist, B.; Liu, B. Uniaxial-stress-driven transformation in cold compressed glassy carbon. *Appl. Phys. Lett.* **2017**, *111*, 101901.
(19) Zeng, Z.; et al. Synthesis of quenchable amorphous diamond. *Nat. Commun.* **2017**, *8*, 322.
(20) Wen, L.; Sun, H. Understanding shear-induced sp^2 -to- sp^3 phase transitions in glassy carbon at low pressure using first-principles calculations. *Phys. Rev. B* **2018**, *98*, 014103.
(21) Yao, M.; Xiao, J.; Fan, X.; Liu, R.; Liu, B. Transparent, superhard amorphous carbon phase from compressing glassy carbon. *Appl. Phys. Lett.* **2014**, *104*, 021916.
(22) Zeng, Z.; Sheng, H.; Yang, L.; Lou, H.; Tan, L.; Prakapenka, V. B.; Greenberg, E.; Zeng, Q. Structural transition in cold-compressed glassy carbon. *Phys. Rev. Mater.* **2019**, *3*, 033608.
(23) Shiell, T. B.; de Tomas, C.; McCulloch, D. G.; McKenzie, D.; Basu, A.; Suarez-Martinez, I.; Marks, N.; Boehler, R.; Haberl, B.; Bradby, J. In situ analysis of the structural transformation of glassy carbon under compression at room temperature. *Phys. Rev. B* **2019**, *99*, 024114.
(24) Shibazaki, Y.; Kono, Y.; Shen, G. Compressed glassy carbon maintaining graphite-like structure with linkage formation between graphene layers. *Sci. Rep.* **2019**, *9*, 7531.
(25) Prescher, C.; Prakapenka, V. B. DIOPTAS: a program for reduction of two-dimensional X-ray diffraction data and data exploration. *High Pressure Res.* **2015**, *35*, 223−230.
(26) Anderson, O. L.; Isaak, D. G.; Yamamoto, S. Anharmonicity and the equation of state for gold. *J. Appl. Phys.* **1989**, *65*, 1534−1543.
(27) Kresse, G.; Hafner, J. Ab initio molecular dynamics for liquid metals. *Phys. Rev. B: Condens. Matter Mater. Phys.* **1993**, *47*, 558−561.
(28) Blöchl, P. E. Projector augmented-wave method. *Phys. Rev. B: Condens. Matter Mater. Phys.* **1994**, *50*, 17953−17979.
(29) Dixon, M.; Hutchinson, P. A method for the extrapolation of pair distribution functions. *Mol. Phys.* **1977**, *33*, 1663−1670.
(30) Zhao, Z.; et al. Nanoarchitectured materials composed of fullerene-like spheroids and disordered graphene layers with tunable mechanical properties. *Nat. Commun.* **2015**, *6*, 6212.
(31) Gaskell, P. H.; Saeed, A.; Chieux, P.; McKenzie, D. R. Neutron-scattering studies of the structure of highly tetrahedral amorphous diamondlike carbon. *Phys. Rev. Lett.* **1991**, *67*, 1286−1289.
(32) Bundy, F. P.; Bassett, W. A.; Weathers, M. S.; Hemley, R. J.; Mao, H. U.; Goncharov, A. F. The pressure-temperature phase and transformation diagram for carbon; updated through 1994. *Carbon* **1996**, *34*, 141−153.